GlidePath: Eco-Friendly Automated Approach and Departure at Signalized Intersections

Osman D. Altan, *Life Member, IEEE*, Guoyuan Wu, *Senior Member, IEEE*, Matthew J. Barth, *Fellow, IEEE*, Kanok Boriboonsomsin, *Member, IEEE*, and John A. Stark

***Abstract*—Recently, there has been significant research on environment-focused connected vehicle (CV) applications that involve determining optimal speed profiles for vehicles traveling through signalized intersections and conveying this information to drivers via driver-vehicle interfaces (DVI's). However, findings from previous studies indicate that drivers may not be able to precisely follow the recommended speed profiles, resulting in degraded effectiveness of the applications. Moreover, the DVI could be distracting, which may compromise safety. As an alternative, *partial automation* can play an important role in ensuring that the benefits of these CV applications are fully realized. In this study, a partially automated vehicle system with an eco-approach and departure feature (called the GlidePath Prototype), which can receive dedicated short range communication message sets from the intersection and automatically follow recommended speed profiles, was developed, demonstrated, and evaluated. The results revealed that compared to manually following the recommended speed profiles, the GlidePath Prototype reduced fuel consumption by 17% on average. In some cases, the fuel savings are greater than 40% while the travel time is shortened by up to 64%. Furthermore, the system potentially improved the driving comfort since it would smooth out the speed profiles.**

***Index Terms*—Connected and automated vehicle (CAV), eco-approach/departure, intelligent transportation systems.**

I. Introduction

With increasing public awareness of the need to reduce carbon emissions and rapid advances in information and communication technology, a significant amount of research has been conducted to develop energy/environment-focused Connected Vehicle (CV) applications. The European Union has initiated a series of programs and projects, such as eCoMove [1] and Compass4D [2], in which traffic information can be shared in real-time among all road users and infrastructure to encourage more efficient and sustainable operations of the entire transportation system. Another good example is the U.S. Department of Transportation's AERIS (Applications for the Environment: Real-Time Information Synthesis) program [3], which aims to develop a variety of CV applications that are specifically designed to reduce the environmental footprint of surface transportation.

Among the CV applications developed under the AERIS program, the Eco-Approach and Departure at Signalized Intersections (EAD) application has shown great promise in terms of reducing fuel consumption and pollutant emissions [4]. Like other CV applications that involve determining optimal speed profiles for vehicles traveling within an urban transportation network (e.g., [5]–[9]), the EAD application utilizes signal phase and timing (SPaT) information from the upcoming traffic signal to determine a recommended speed profile that minimizes vehicle energy consumption and pollutant emissions when approaching to and departing from a signalized intersection. The recommended speed profile is then conveyed to the driver through driver-vehicle interfaces (DVI's). However, the driver may not be able to precisely follow the recommended speed profile [11], resulting in degraded effectiveness of the application. Furthermore, these DVIs could be distracting, which may compromise safety.

In this respect, partial vehicle automation, even at Level 1 (function-specific automation) or Level 2 (combined function automation) [10], can play an important role in better following the recommended speed profiles, thereby ensuring that the benefits of the EAD application are fully realized. In [11], a numerical simulation study was conducted to quantify the supplementary benefits from partial vehicle automation. As a continuation of research in [11], a partially automated version of the EAD application, called GlidePath Prototype, has been developed, demonstrated, and evaluated in this study. The GlidePath Prototype system is the first of its kind, integrating state-of-the-art connected vehicle and automated vehicle control technologies.

The remainder of this paper is organized as follows: Section II presents background information on vehicle movement at signalized intersections and the associated energy consumption. The core algorithm of the GlidePath Prototype system—vehicle trajectory planning—is then elaborated in Section III. Next, detailed description of the GlidePath experiment as well as

Manuscript received June 17, 2016; revised May 9, 2017 and July 30, 2017; accepted September 22, 2017. Date of publication November 3, 2017; date of current version December 18, 2017. This work was supported by the Federal Highway Administration and was performed with Leidos Inc. *(Corresponding author: Guoyuan Wu.)*

O. D. Altan is with the Turner Fairbank Highway Research Center, Federal Highway Administration, U.S. Department of Transportation, McLean, VA 22101 USA (e-mail: osman.altan@dot.gov).

G. Wu and K. Boriboonsomsin are with the College of Engineering—Center for Environmental Research and Technology, University of California, Riverside, Riverside, CA 92507 USA (e-mail: gywu@cert.ucr.edu; kanok@cert.ucr.edu).

M. J. Barth is with the College of Engineering—Center for Environmental Research and Technology and the Department of Electrical and Computer Engineering, University of California, Riverside, Riverside, CA 92507 USA (e-mail: barth@ece.ucr.edu).

J. A. Stark is with Leidos, Inc., Reston, VA 20190 USA (e-mail: JOHN.A.STARK@leidos.com).

Color versions of one or more of the figures in this paper are available online at http://ieeexplore.ieee.org.

Digital Object Identifier 10.1109/TIV.2017.2767289

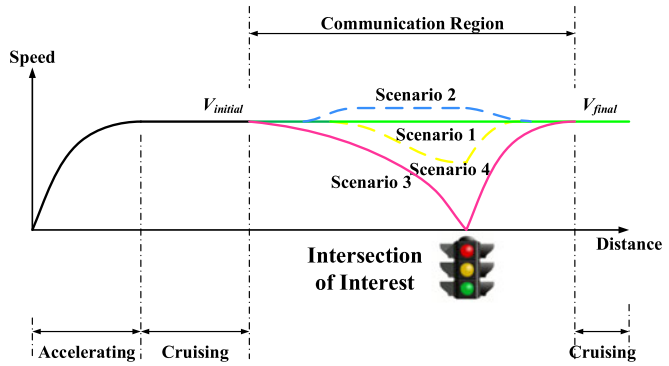

Fig. 1. Illustration of different scenarios for a vehicle approaching a signalized intersection.

data collection efforts are presented in Section IV, followed by comparative analyses of the collected data (for both manual and partially automated driving) and discussion of the results in Section V. Lastly, Section VI concludes this paper along with further discussion on future work.

II. Background

A. Vehicle Movements at Isolated Intersections

For signalized arterials, consider the scenario of a single traffic light as shown in Fig. 1. In this figure, velocity trajectories of four different vehicles confronted with the traffic light at different signal phases and timings are shown by the green, blue, red, and yellow lines. Note that all these trajectories have the same initial and final velocities, and the same traveled distance (e.g., within the dedicated short range communication (DSRC) range). More specifically, the scenario can be divided into the following four cases:

1) Scenario 1 ("cruise"): The vehicle cruises through the intersection with constant speed (green line);
2) Scenario 2 ("speed-up"): The vehicle speeds up to pass the intersection and then gets back to the initial speed after the intersection (blue line);
3) Scenario 3 ("coast-down with a full stop"): The vehicle slows down and stops at the intersection (red line);
4) Scenario 4 ("coast-down without a full stop" or "glide"): The vehicle slows down and passes the intersection with a mid-range speed, and then speeds up to its initial speed (yellow line).

Even though all these vehicles cover the same distance with the identical initial and final velocities, the associated fuel consumption and emissions may vary greatly. Generally speaking, Scenario 3 likely uses the most amount of fuel as the vehicle has to decelerate to a full stop, idle for a certain period, and then accelerate from stop to the final velocity. However, fuel consumption of Scenario 1 may be comparable to that of Scenario 2 and/or Scenario 4, depending on detailed maneuvers (e.g., acceleration rate, top speed, duration) under each driving modes (i.e., acceleration, cruise, and deceleration) during the trips.

Therefore, as a vehicle travels down a signalized corridor, it would likely be better to speed up or slowdown a moderate amount in advance if maintaining current speed will not allow itself to pass through the intersection within the green phase. As the vehicle approaches a signal, its velocity can be dynamically adjusted to minimize fuel consumption and emissions. This is the basic idea behind the vehicle trajectory planning algorithm proposed in [11] and deployed in this study.

B. Eco-Driving Along Urban Arterial

Over the years, a variety of eco-driving strategies have been developed to improve the energy efficiency for traveling along signalized intersections in the urban area [5]–[9], [11], [12]. For example, Ozatay *et al*. proposed eco-driving algorithms with analytical and/or numerical solutions that can minimize the fuel consumption for vehicles passing through signalized corridors [22], [23]. He *et al*. considered the queue effect at signalized intersections when planning the vehicle trajectory for fuel efficient driving [24]. A recent study by Jin *et al*. took the "bottom-up" approach, i.e., selecting the best powertrain operation state at each time step while satisfying the exogenous constraints (e.g., preceding vehicle movement, traffic signal control), and formulated the problem into a mixed integer linear program in order to obtain the vehicle dynamics that minimize the fuel consumption for urban driving [25]. In addition, results from the numerical simulation study show that the "bottom-up" approach outperformed some existing algorithms in terms of energy savings. Some other studies focus on the development or evaluation eco-driving strategies from the perspective of traffic flows [26]. Besides the research on traditional fossil fueled vehicles, more and more studies have been focused on the development of eco-driving strategies for alternative fueled vehicles, such as hybrid electric vehicles, battery electric vehicles. They applied various optimization strategies, including Dynamic Programming [27] and Pontryagin's Minimum Principle [28], to obtaining the most energy efficient speed profiles in consideration of some unique features (e.g., regenerative braking).

However, most of these strategies (especially from the partially automated perspective) were only tested in the simulation environment (i.e., using vehicle simulators, driving simulators or microscopic traffic simulators). And some of them could be too computationally demanding to be deployed in the field. In this study, our proposed vehicle trajectory planning algorithm was validated in a real world system.

C. Comprehensive Modal Emissions Model (CMEM)

In this study, the Comprehensive Modal Emissions Model (CMEM) [13] is used to accurately assess the fuel consumption and emissions of each run of the experiment ground vehicle (XGV). CMEM is a microscopic emissions model that is capable of predicting second-by-second fuel consumption and tailpipe emissions of carbon dioxide (CO2), carbon monoxide (CO), hydrocarbons (HC), and nitrogen oxides (NOx) based on different modal operations from an in-use vehicle fleet. In the modeling approach of CMEM, the entire fuel consumption and emissions process is broken down into components that correspond to physical phenomena associated with vehicle operation and emissions production, as represented by the following key

equations:

$$P_{tr} = \max\{M \cdot v \cdot (a + g \cdot \sin\theta) + (M \cdot g \cdot C_r + \frac{\rho}{2} \cdot v^2 \cdot A \cdot C_a) \cdot v,\ 0\} \quad (1)$$

$$P_{\text{eng}} = P_{tr}/\eta_{tf} + P_{\text{acc}} \quad (2)$$

$$Fuelrate \approx \phi \cdot \left(k \cdot N \cdot D + \frac{P_{\text{eng}}}{\eta_{\text{eng}}}\right) \cdot \frac{1}{44} \quad (3)$$

$$Emissions_{\text{tailpipe}} = Fuelrate \cdot \frac{g_{\text{emissions}}}{g_{\text{fuel}}} \cdot CPF \quad (4)$$

where P_{tr} is the tractive power (kW); M is the vehicle mass (kg); v is the vehicle velocity (m/s); a is the vehicle acceleration (m/s^2); g is the gravitational constant (i.e., 9.81 m/s^2); θ is the road grade angle (in fraction); C_r is the rolling resistance coefficient; ρ is the mass density of air (i.e., 1.225 kg/m^3, depending on temperature and altitude); A is the vehicle cross sectional area (m^2); C_a is the aerodynamic drag coefficient; P_{eng} is the engine power (kW); η_{tf} is the combined efficiency of the transmission and final drive; P_{acc} is the power demand (kW) associated with the operation of accessories, such as air conditioning, power steering and brakes, and other electrical loads; ϕ is the fuel/air equivalence ratio; 44 (kJ/g) is the lower heating value of a typical gasoline; k is the engine friction factor, representing the fuel energy used at zero power output to overcome engine friction per engine revolution and unit of engine displacement); N is the engine speed (revolutions per second); D is the engine displacement (litre); η_{eng} is the indicated engine efficiency; $(g_{\text{emissions}}/g_{\text{fuel}})$ is the engine-out emissions per unit of fuel consumed; and CPF is the catalyst pass fraction, which is defined as the ratio of tailpipe to engine-out emissions. *CPF* usually is primarily a function of fuel/air ratio and engine-out emissions.

Each component of CMEM is modeled as an analytical representation consisting of various parameters that are characteristic of the process. These parameters vary according to vehicle type, engine, emission control technology, and level of deterioration. Some of them are available from the public resources or specifications (e.g., engine displacement), while others are measured or calibrated in the dedicated facilities [13]. CMEM has been developed primarily for microscale transportation models that typically produce second-by-second vehicle trajectories (location, velocity, and acceleration). These vehicle trajectories can be applied directly to the model, resulting in both individual and aggregate energy/emissions estimates.

III. Vehicle Trajectory Planning Algorithm and its Components

At the core of the GlidePath Prototype system, Vehicle Trajectory Planning Algorithm (VTPA) is responsible for generating the reference speed trajectory as the input to the longitudinal controller.

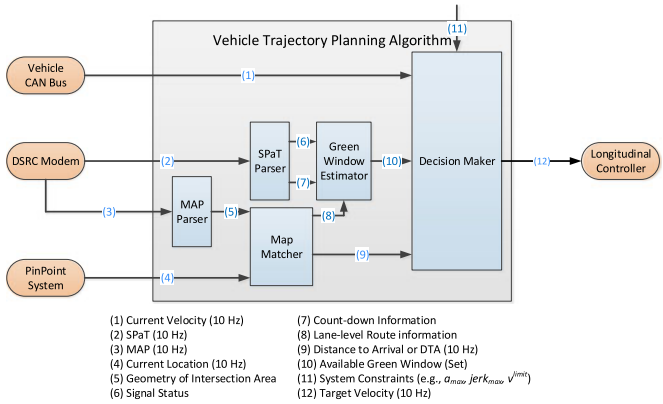

Fig. 2. Sub-systems of VTPA.

A. Vehicle Trajectory Planning Algorithm (VTPA)

Fig. 2 depicts the system diagram of the vehicle trajectory planning algorithm (VTPA), where external inputs include:

1) Vehicle's current states, such as location (i.e., latitude, longitude and altitude) received from the PinPoint system [20] and instantaneous velocity obtained from the vehicle CAN Bus interface. It turns out the PinPoint system can provide quite precise location information (up to the centimeter level) of the test vehicle in this study;
2) Message sets received from the DSRC device, which include SPaT and MAP (also referred to as geometric intersection description or GID) messages; and
3) System constraints and parameters, such as maximum acceleration and deceleration, maximum jerk (i.e., derivative of acceleration), and roadway speed limit.

The output is the target velocity. A further insight into the VTPA system shows there are five sub-systems:

1) *MAP Parser*: by following SAE J2735 protocol [21], this sub-system can decode the MAP messages broadcasted by the road-side equipment (RSE) and extract the characteristics of key nodes at/around the intersection, such as latitudes, longitudes and elevations along each approach and departure lane;
2) *Map Matcher*: based on the vehicle's current location, stop-bar location, and locations of those key nodes in-between, this sub-system can compute the lane ID and the vehicle's distance to the stop-bar or distance-to-arrival (DTA) at each time step;
3) *SPaT Parser*: Also by following SAE J2735 protocol, this sub-system can decode the SPaT messages broadcasted by the RSE and extract the current signal status (i.e., green/yellow/red and solid/arrow) applicable to the current lane as well as the range (the minimum and maximum) of count-down to the end of current status;
4) *Green Window Estimator*: this sub-system aims at estimating available green windows for the subject vehicle according to the vehicle's desired movement, SPaT and signal controller's type (e.g., fixed-time or traffic-responsive) and settings. For a fixed-time signal controller, it is quite easy and robust to estimate green windows due to its simple control logic. But for a traffic-response signal

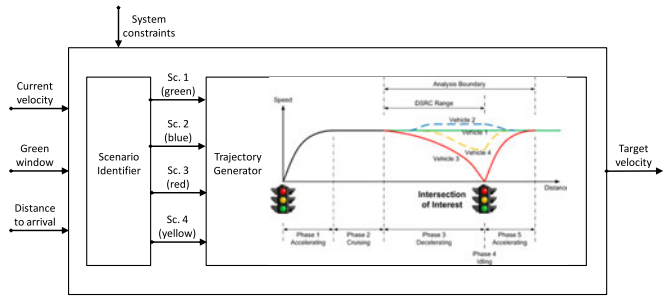

Fig. 3. Diagram of the decision maker sub-system.

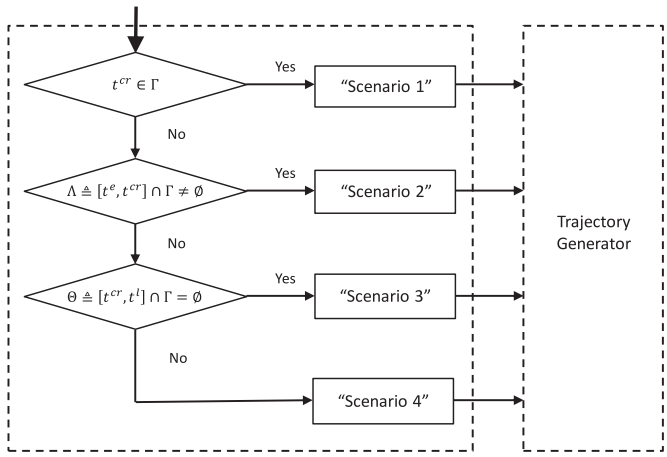

Fig. 4. Diagram of scenario identifier.

controller, more advanced statistical techniques need to be employed to obtain relatively more reliable estimation of green windows, depending on the degree of actuation [14].

5) *Decision Maker*: this sub-system takes into account the holistic information, including system constraints (e.g., maximum acceleration/deceleration, roadway speed limit,), to identify the scenario (see Section II-B) where the subject vehicle faces and determines the appropriate target speed profile. As shown in Fig. 3, this sub-system consists of two components: 1) Scenario Identifier; and 2) Trajectory Generator.

B. Scenario Identifier

As shown in Fig. 4, the Scenario Identifier component is to identify into which scenario the target vehicle trajectory should be categorized, based on some key parameters (such as speed, SPaT, distance to stop bar and other system constraints) at current time. For example, if the subject vehicle can cruise at the current velocity and pass the intersection at green, then the trajectory is categorized into Scenario 1 (cruise), and the cruise time to arrival, t^{cr}, is given as

$$t^{cr} = d_0 / v_c \tag{5}$$

where d_0 is the route distance to the stop-bar and v_c is the instantaneous speed at current time instant, t_0. In addition, the available green window, Γ, can be written as follows:

$$\Gamma = \begin{cases} [t_0, g_e^{\text{curr}}) \cup [g_s^{\text{next}}, g_e^{\text{next}}) \ , & \text{if } \text{"Green"} \ at \ t_0 \\ [g_s^{\text{next}}, g_e^{\text{next}}) \ , & \text{if "Yellow"} \ or \ \text{"Red"} \ \text{at} \ t_0 \end{cases} \tag{6}$$

where g_e^{curr} denotes the end of current green window associated with the vehicle's movement; g_s^{next} and g_e^{next} represent the start and end of next green window, respectively. Generally speaking, Γ should be the set of all subsequent green windows after t_0. But within the limited communication range of DSRC (300 meters, nominally), the time window up to the end of next green should be practically long enough to tackle with most situations. For some extreme situations, e.g., over-saturated traffic conditions, the green windows after the next cycle can be included in Γ (in theory), but it is very likely that the vehicle has to stop due to the long queue effect.

If Scenario 1 is not guaranteed, then the earliest time to arrival, $t^e (< t^{cr})$, will be calculated to determine whether the trajectory satisfies the condition of Scenario 2, i.e., speed-up (without violating the speed limit) to pass through the signal without any stop. The calculation of t^e largely depends on the proposed trajectory model, a piecewise trigonometric-linear function, which will be elaborated in the following section.

If it is determined that the subject vehicle will not be able to pass the intersection by moderate acceleration, then the vehicle has to decelerate to a full stop (Scenario 3) or to glide in an environmentally friendly manner (Scenario 4), depending on the latest time to arrival without any stop, $t^l (> t^{cr})$. Again, the calculation of t^l is model-dependent.

C. Trajectory Generator

This component is to determine the actual time-to-arrival, t^{arr} (for Scenario 3, it is the time instant to leave from the stop-bar), and the target vehicle trajectory for each scenario. As mentioned in Section II, the proposed control logic for the target velocity tries to minimize the vehicle's acceleration/ deceleration before the intersection, so that the vehicle can pass the intersection with the target speed that is closest to its initial speed (assuming it is the free-flow speed). Therefore, after passing the intersection, the vehicle can get back to its initial speed with minimal fuel usage. As suggested in previous literature [15], [16], there are numerous ways to accelerate or decelerate from one speed to another, such as the constant acceleration and deceleration rates, linear acceleration and deceleration rates, and constant power rates. The family of piecewise trigonometric-linear functions is selected as the target velocity profiles (for both approach and departure portions), due to its mathematical tractability and smoothness [17].

The basic idea for our generated trajectory is: the acceleration and deceleration are designed to achieve the desired cruise speed in the shortest amount of time, while ensuring the driving comfort by limiting the jerk. In order to avoid unnecessary idling, the vehicle tries to reach the intersection during the green phase of the signal.

For Scenario 1, since the vehicle is able to cruise through the intersection, the time-to-arrival, $t^{\text{arr}} = t^{cr}$, and the target

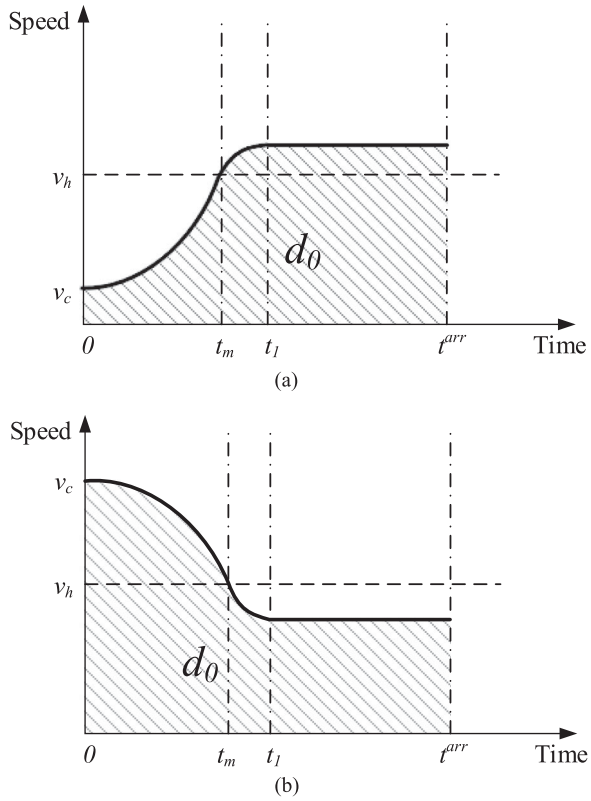

Fig. 5. (a) Acceleration profile of the piecewise trigonometric-linear function. (b) Deceleration profile of the piecewise trigonometric-linear function.

velocity, v_t, is simply the current velocity (at $t = 0$, without loss of generality), v_c.

For Scenario 2, the approach portion takes the similar shape of acceleration profile in Fig. 5(a). To reach back to v_c after passing the signal, the departure portion is the mirror symmetry of the approach one for simplicity. More specifically, without compromising the travel time, the time-to-arrival is given as

$$t^{\text{arr}} = \min \Lambda \triangleq \min \{[t^e,\ t^{cr}] \cap \Gamma\} \tag{7}$$

The target velocity, $v_t = f(t|v_c,\ v_h)$, where

$$f\left(t|v_c, v_h\right) = \begin{cases} v_h - v_d \cdot \cos\left(mt\right) & t \in \left[0,\ \dfrac{\pi}{2m}\right) \\ v_h - v_d \cdot \dfrac{m}{n} \cdot \cos\left[n \cdot \left(t + \dfrac{\pi}{n} - t_1\right)\right] & t \in \left[\dfrac{\pi}{2m},\ t_1\right) \\ v_h + v_d \cdot \dfrac{m}{n} & t \in \left[t_1,\ \dfrac{d_0}{v_h}\right) \\ v_h - v_d \cdot \dfrac{m}{n} \cdot \cos\left[n \cdot \left(t + \dfrac{3\pi}{2n} - t_2\right)\right] & t \in \left[\dfrac{d_0}{v_h},\ t_2\right) \\ v_h - v_d \cdot \cos\left[m \cdot (t - t_3)\right] & t \in \left[t_2, t_3\right) \\ v_c & t \in \left[t_3,\ +\infty\right) \end{cases} \tag{8}$$

and $n\ (> 0)$ is chosen as the maximum that satisfies:

$$\begin{cases} |n \cdot v_d| \le a_{\max} \\ |n \cdot v_d| \le d_{\max} \\ |n^2 \cdot v_d| \le jerk_{\max} \\ n \ge \left(\dfrac{\pi}{2} - 1\right) \cdot \dfrac{v_h}{d_0} \end{cases} \tag{9}$$

and,

$$m = \frac{-\frac{\pi}{2}n - \sqrt{\left(\frac{\pi}{2}n\right)^2 - 4n^2 \cdot \left[\left(\frac{\pi}{2} - 1\right) - \frac{d_0}{v_h} \cdot n\right]}}{2\left[\left(\frac{\pi}{2} - 1\right) - \frac{d_0}{v_h} \cdot n\right]} \tag{10}$$

where $v_h = d_0/t^{\text{arr}}$, representing the target average speed given target arrival time, t^{arr}; $v_d = v_h - v_c$, representing the difference between current speed and target average speed; $t_1 = \pi/2m + \pi/(2n)$; $t_2 = d_0/v_h + \pi/(2n)$; $t_3 = d_0/v_h + \pi/(2m) + \pi/(2n)$; $a_{\max}$ and $d_{\max}$ are the maximum acceleration and deceleration, respectively; $|jerk_{\max}| = 10$ m/s^3 is the maximum jerk whose value was chosen as recommended in [18]; The parameters m and n define the family of trigonometric functions, whose values control the rate of change in acceleration and deceleration profiles. In addition, the parameters m and n are coupled in order to guarantee the smoothness of entire speed profile (especially at those break points) and the area under the curve being the distance to the stop-bar, d_0.

According to the Equation Set (8), the earliest time-to-arrival, t^e, can be calculated as

$$t^e = \frac{d_0 - v_c \cdot \frac{\pi}{2p}}{v^{\text{limit}}} + \frac{\pi}{2p} \tag{11}$$

and

$$p = \min\left\{\frac{2 \cdot a_{\max}}{v^{\text{limit}} - v_c}, \sqrt{\frac{2 \cdot jerk_{\max}}{v^{\text{limit}} - v_c}}\right\} \tag{12}$$

where, v^{limit} represents the upper limit (hard constraint) of the target velocity due to the subject vehicle's ability or roadway enforcement.

As aforementioned, to determine if the speed profile belongs to Scenario 3 or Scenario 4, the latest time-to-arrival without any stop, t^l, can be calculated as

$$t^l = \frac{d_0 - v_c \cdot \frac{\pi}{2q}}{v^{\text{coast}}} + \frac{\pi}{2q} \tag{13}$$

and

$$q = \min\left\{\frac{2 \cdot a_{\max}}{v_c - v^{\text{coast}}}, \sqrt{\frac{2 \cdot jerk_{\max}}{v_c - v^{\text{coast}}}}\right\} \tag{14}$$

where v^{coast} denotes the coasting speed (e.g., 8 mph) which is a user-defined parameters based on driving comfort.

For Scenario 3, since the vehicle needs to have a full stop at the stop-bar, the time-to-arrival is not equal to the time to leave from the stop-bar, or $t^{\text{arr}} < g_s^{\text{next}}$ and the target velocity,

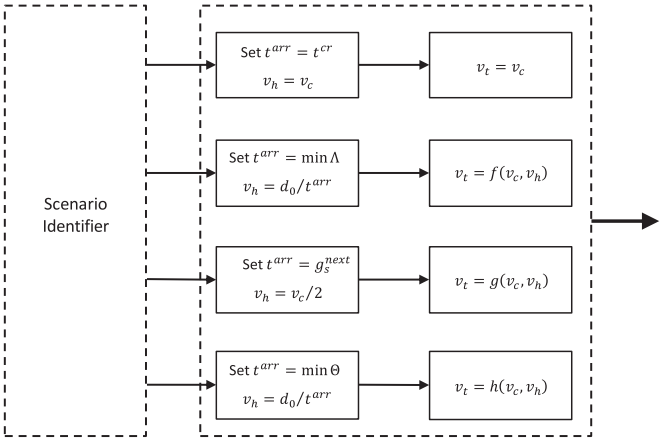

Fig. 6. Diagram of trajectory generator.

$v_t = g(t|v_c,\ v_h)$, where

$$g\left(t|v_c, v_h\right) = \begin{cases} v_h - v_d \cdot \cos\left(mt\right) & t \in \left[0,\ \dfrac{\pi}{2m}\right) \\ v_h - v_d \cdot \dfrac{m}{n} \cdot \cos\left[n \cdot \left(t + \dfrac{\pi}{n} - t_1\right)\right] & t \in \left[\dfrac{\pi}{2m},\ t_1\right) \\ v_h + v_d \cdot \dfrac{m}{n} & t \in \left[t_1,\ g_s^{\text{next}}\right) \\ v_h - v_d \cdot \dfrac{m}{n} \cdot \cos\left[n \cdot \left(t + \dfrac{3\pi}{2n} - t_4\right)\right] & t \in \left[g_s^{\text{next}},\ t_4\right) \\ v_h - v_d \cdot \cos\left[m \cdot (t - t_5)\right] & t \in \left[t_4, t_5\right) \\ v_c & t \in \left[t_5,\ +\infty\right) \end{cases} \tag{15}$$

and,

$$n = m = \frac{v_h}{d_0} \cdot \pi \tag{16}$$

where $t_4 = g_s^{\text{next}} + \pi/(2n)$; $t_5 = t_4 + \pi/(2m)$ and $v_h = v_c/2$; Due to (16), Equation Set (15) can be further simplified as

$$\begin{cases} v_c/2 + v_c/2 \cdot \cos\left(mt\right) & t \in \left[0,\ t^{\text{arr}}\right) \\ 0 & t \in \left[t^{\text{arr}},\ g_s^{\text{next}}\right) \\ v_c/2 + v_c/2 \cdot \cos\left[m \cdot (t - t_5)\right] & t \in \left[g_s^{\text{next}},\ t_5\right) \\ v_c & t \in \left[t_5,\ +\infty\right) \end{cases} \tag{17}$$

For Scenario 4, the time-to-arrival is given as

$$t^{\text{arr}} = \min \Theta \triangleq \min\left\{\left[t^{cr}, t^{l}\right] \cap \Gamma\right\} \tag{18}$$

And the target velocity, $v_t = h(t|v_c,\ v_h)$ shares the same format of $f(t|v_c,\ v_h)$, but $v_d < 0$. Fig. 6 summarizes how to determine the time-to-arrival, t^{arr}, the average speed, v_h, and the target speed, v_t, for each of the four scenarios.

IV. GlidePath Testbed and Data Collection

In this section, the GlidePath testbed and field experiment for data collection will be described in detail. Fig. 7 illustrates all sub-systems of the GlidePath testbed, including GlidePath Prototype (i.e., experiment ground vehicle or XGV) and relevant roadside infrastructure.

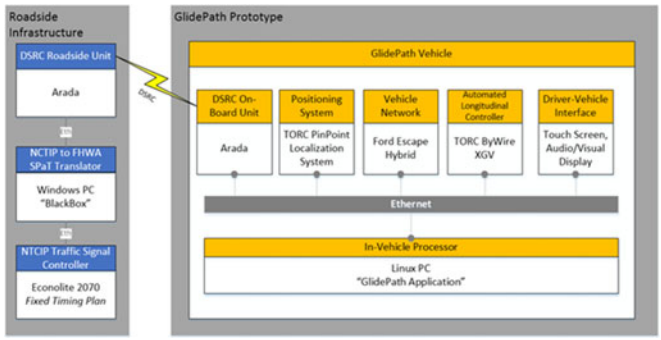

Fig. 7. Sub-systems of GlidePath testbed.

Fig. 8. XGV setup and driver-vehicle interface (DVI).

A. GlidePath Prototype

The GlidePath prototype is a 2010 Ford Escape Hybrid outfitted by TORC Robotics with ByWire XGV System, enabling full-range longitudinal speed control (see Fig. 8). Other key components or functionalities integrated into the test vehicle include: 1) DSRC on-board equipment (OBE); 2) advanced positioning system; 3) driver-vehicle interface; 4) emergency stop and manual override; and 5) data logging.

The GlidePath Prototype and its subsystems can be controlled by several input mechanisms that, in combination, serve as transitions between the vehicle states which are depicted in Fig. 9.

B. Test Site

The field test was conducted at the Turner-Fairbank Highway Research Center (TFHRC) in McLean, Virginia using the Saxton Lab Intelligent Intersection, which offered a sheltered traffic environment where the automated prototype was able to be tested with minimal safety risk and without disrupting live traffic operations.

Fig. 10 provides an overview of the field test site, specifying starting point where the vehicle will begin test runs from a

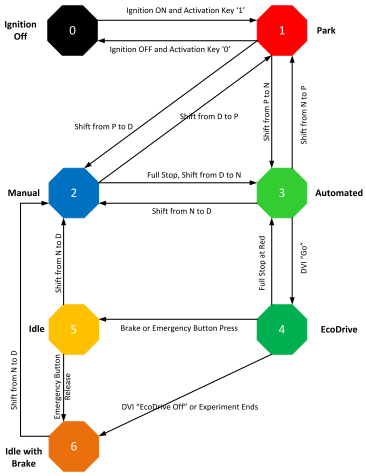

State Description		
No.	Name	Automated Control
0	Ignition off	Disabled
1	Park	Disabled
2	Manual	Disabled
3	Automated	Enabled
4	EcoDrive	Actively Engaged
5	Idle	Disabled
6	Idle with brake	Disabled

Fig. 9. GlidePath prototype system state transition diagram.

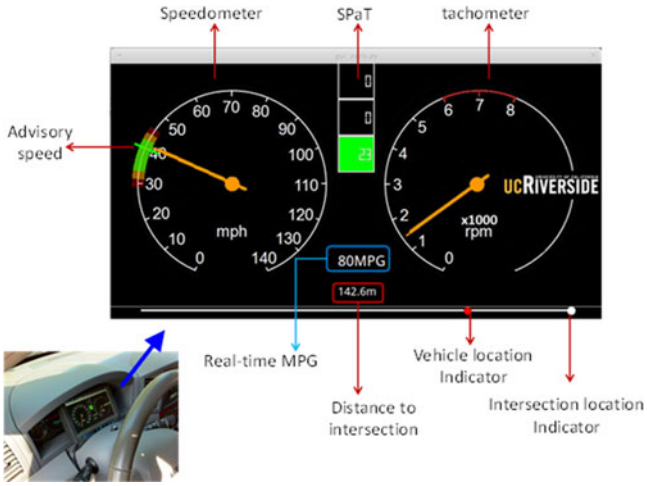

Fig. 11. Graphic interface for "manual-DVI-assisted" driving.

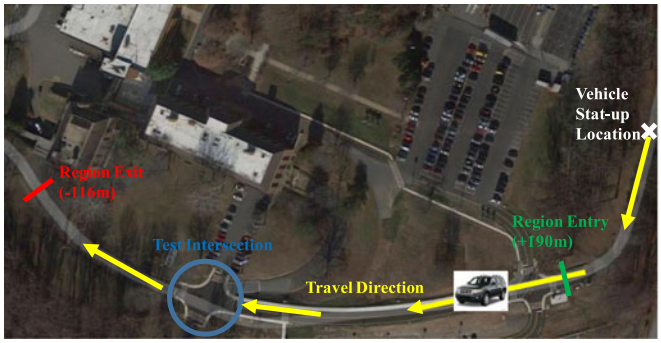

Fig. 10. Field study site in Turner Fairbank Highway Research Center in McLean, VA.

stop and travel westbound towards the intersection and relevant roadside infrastructure (including an Econolite 2070 controller, Windows PC to encode SPaT and MAP messages, and Arada Locomate DSRC Roadside Unit). The test zone covers a range from 190 meters to the east of the intersection to 116 meters to the west, which allows a maximum traveling speed of up to 30 mph. The traffic signal controller was set up for fixed timed signal plan: 27-seconds green, 3-seconds yellow, followed by 30-seconds of red, which has removed excess all red clearance timings and all loop detector triggers from actuating the signal.

C. Data Collection

The field experiment was designed to be comprehensive in that the test vehicle will approach the intersection at different times throughout the entire signal cycle (i.e., every 5 seconds in the 60-second cycle). Furthermore, the vehicle approached the intersection at different driving speeds (i.e., operating speeds), ranging from 20 mph to 25 mph. The limitations of the TFHRC facility roadway prevent use of higher operating speeds. The vehicle fuel economy and CO2 emissions were then calculated by applying the CMEM model to the logged trajectories, and compared between the following stages:

1) Stage I: *"manual-uninformed" driving:* At this stage, a driver approached and traveled through the intersection in a normal fashion without guidance or automation, stopping as needed without any automated vehicle control. Data collected at this stage establish a baseline that can be used as a point of comparison for the Stage II and III experiments.
2) Stage II: *"manual-DVI-assisted" driving:* At this stage, a driver was provided an enhanced dashboard which presented a speed range band overlaid onto a speedometer for the driver to follow as guidance on how to approach and depart the intersection in an environmentally friendly manner while obeying the traffic signal (see Fig. 11). This stage does not involve any automated vehicle control but the advisory speed trajectories were generated using VTPA described previously. In addition, the recommended speed profile can be re-calculated throughout the route if the subject cannot follow the recommendation well enough (i.e., the accumulative following error reaches some user-defined threshold). Such mechanism may trigger the change from one scenario to another en-route.
3) Stage III: *"(partially) automated" driving:* At this stage, the developed GlidePath prototype system was responsible for longitudinal control of the vehicle allowing it to speed up or slow down while the driver steered for lateral control and monitored the application on the DVI (shown in Fig. 12). At this stage, the vehicle automatically controlled the brake and throttle based on the output of the Vehicle Trajectory Planning Algorithm (VTPA), which calculated an eco-friendly velocity profile according to the DSRC message sets and distance to the stop-bar. Fig. 13 presents an example of the actual speed vs. reference speed (i.e., the controlled input) to show the tracking performance of the longitudinal controller. System parameters were adjusted to accommodate the tracking errors and delay.

Fig. 12. Graphic interface for "(partially) automated" driving.

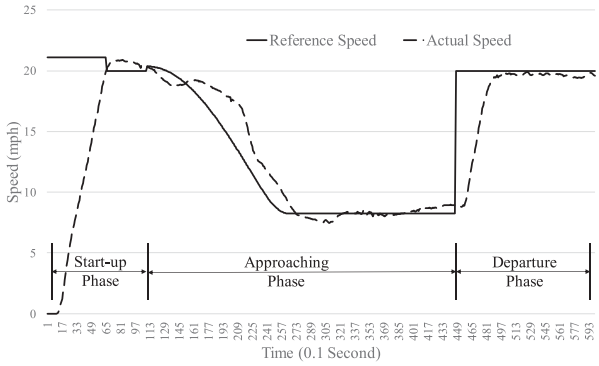

Fig. 13. Example of actual speed vs. reference speed in the field test (when the operating speed is 20 mph and the entry time in phase is 27 seconds after the green on-set).

For the Stage I and Stage II experiments, four drivers who had no previous exposure to the Eco-Approach and Departure concept were recruited to conduct test runs. For the Stage III experiments, the test vehicle was operated by a trained driver to maintain safety as a top priority. Because the GlidePath prototype system can automatically control the longitudinal motion of the vehicle, it is not necessary for novice drivers to operate the vehicle during the "(partially) automated" driving stage.

In order to cover every possible driving scenario (as mentioned in Section II), a field study matrix (i.e., Table I) that varies the vehicle's operating speed and signal timing start with respect to the overall cycle of the traffic signal, was developed for each driver at each stage. This test matrix consists of the operating speed along the vertical axis, and the delay in the signal cycle across the horizontal access as well as the expected current phase of the traffic signal. In this matrix, there are a total of 12 (intervals) $\times$ 2 (speed levels) $=$ 24 test cells. For the experiments, the drivers had to drive through the intersection at least once in order to fill out the field study matrix for each cell. Therefore, a total of 24 (test cells) $\times$ 2 (manual stages) $\times$ 4 (drivers) $+$ 24 (test cells) $\times$ 1 (automated stage) $=$ 216 test runs were conducted. For each data run, key data elements were logged at 10 Hz and post-processed to determine energy consumption and other performance measures.

V. Results and Analyses

Due to the applicability of the CMEM model, results in this Section are based on the second-by-second trajectories aggregated from higher resolution (e.g., 10 Hz) data. Comparative studies between different stages have been conducted on a test cell basis and on a scenario basis, respectively. Both environmental sustainability and mobility will be evaluated here.

A. Test Cell-Based Comparison

As aforementioned, field study matrices have been created to facilitate the presentation of test results. Since there are multiple drivers involved in the data collection for Stage I and Stage II, aggregated statistics (e.g., mean, standard deviation, and median) are calculated for comparison. As noted in [19], median is more robust than mean. Therefore, the following evaluation will focus on the medians of performance measures.

1) Fuel Consumption and Emissions: Table I summarizes results on fuel consumption per distance for different stages at different operating speeds, based on the estimation from CMEM. As shown in the table, Stage III ("automated" driving) outperforms (on average) either Stage I ("manual-uninformed" driving) or Stage II ("manual-DVI-assisted" driving) in terms of fuel consumption at different operating speeds. Stage II performs (on average) better than Stage I when operating speed is 25 mph but there is trivial difference between them in the case of 20 mph. To gain further insight, each cell is colored based on scenario (i.e., "cruise", "speed-up", "coast-down with stop", and "glide") into which the test run sample is categorized. It can be observed that:

1) Scenario 2 ("speed-up") occurred for Stage III but neither for Stage I (no information on when the phase will change) nor Stage II. The reason is that the "median" driver at Stage II could not closely follow the speed advice at the beginning, therefore the recalculation mechanism triggered the change in scenario from 2 to 3 ("coast-down with stop").
2) Scenario 3 **never** occurred for Stage III under the settings in this study. But with shorter approach portion, longer red phase and higher coasting speed, "automated" driving may still have to experience a full-stop scenario.
3) Further investigation on cells of "Green 7" (at 20 mph of operating speed) reveals that, the "median" driver at Stage I barely passed through the intersection at yellow (labeled as Scenario I) while the "median" driver at Stage II failed to follow the recommendation well enough and missed the "speed-up and pass" opportunity even with DVI-assistance (scenario changed from 2 to 3 en-route).

To better evaluate the improvement in fuel economy for the GlidePath Prototype system, relative changes (from one stage to another) are calculated and shown in Figs. 14(a) and 14(b). As can be seen from the figures, Stage III can, on average, save about 18%–20% fuel (but varying from 2% to 46%), compared to Stage I at different operating speed. The performance of Stage II significantly varies with operating speed. For example, Stage II consumed 8% less fuel than Stage I at 25 mph, but it required 4% more fuel consumption at 20 mph.

TABLE I
MEDIAN OF NORMALIZED (BY DISTANCE) FUEL CONSUMPTION (ACROSS ALL DRIVERS) FOR EACH TEST CELL (GRAM/MILE)

Speed (mph)	Phase	Green						Red						Avg.
	TIP[a]	2	7	12	17	22	27	2	7	12	17	22	27	
20	I[b]	58.1	60.9	143.1	135.7	126.7	126.2	126.5	111.6	57.9	56.6	60.2	61.1	93.7
	II[c]	63.8	111.1	137.3	128.0	116.4	122.0	122.8	80.8	61.5	57.0	60.9	60.3	93.5
	III[d]	54.5	56.1	92.4	107.8	101.6	92.8	80.9	59.8	56.8	51.8	51.4	53.6	71.6
25	I	62.1	55.3	159.6	157.2	153.8	146.2	141.1	136.5	109.1	58.2	60.3	59.5	108.2
	II	54.7	58.7	144.5	148.5	140.1	138.7	139.2	130.9	71.3	55.3	53.8	55.2	99.2
	III	48.4	50.0	97.2	142.1	134.4	132.1	130.3	97.5	75.3	49.3	49.1	46.7	87.7

[a] Time-In-Phase when the test vehicle entered the region (i.e., 190 meters to the stop-bar);
[b] Stage I: "manual-uninformed" driving;
[c] Stage II: "manual-DVI-assisted" driving;
[d] Stage III: "automated" driving. For this stage, there is only one run in each cell.

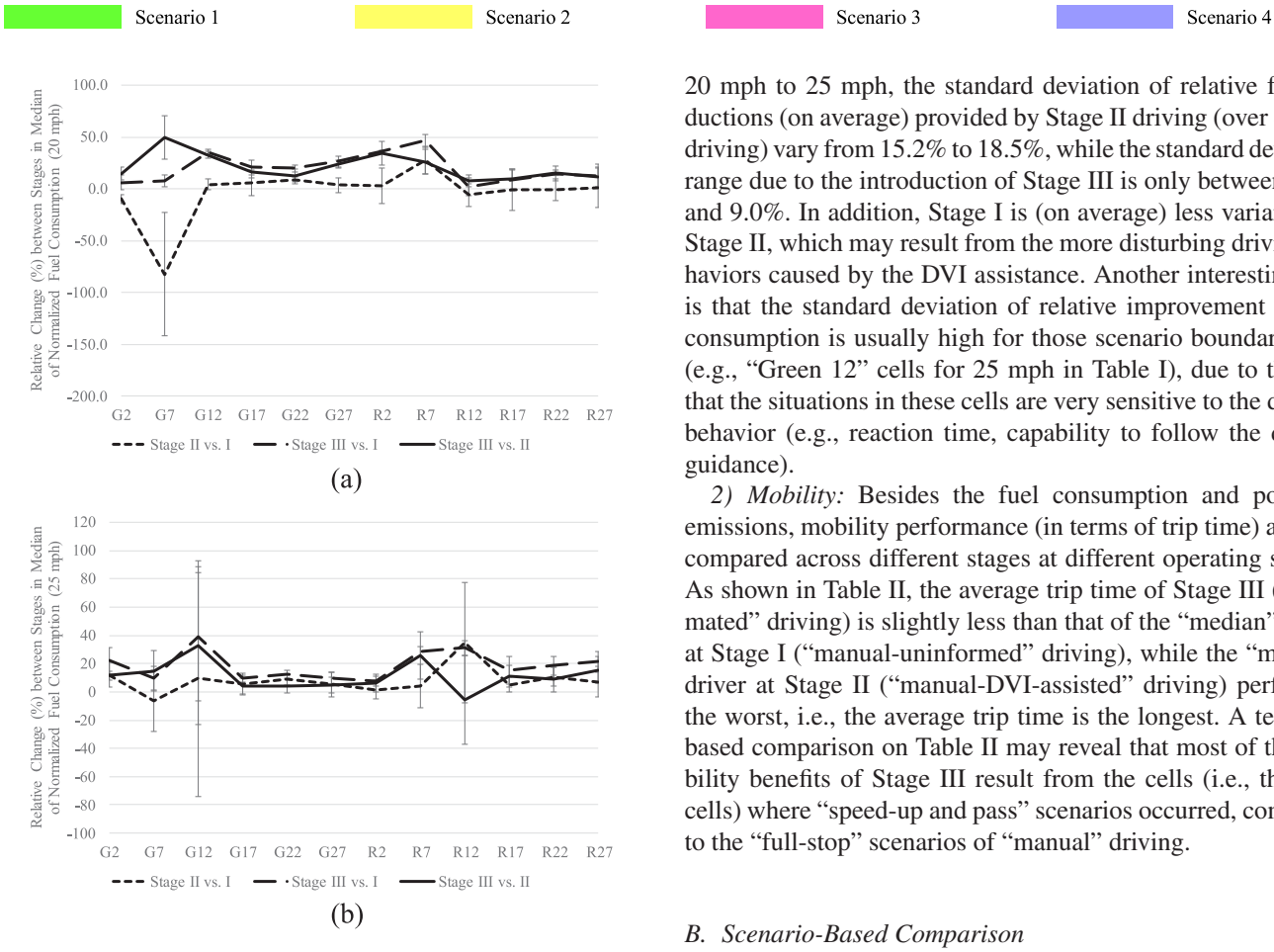

Fig. 14. (a) Relative change (%) between stages (and standard deviation) in median of normalized fuel consumption across all drivers (operating speed is 20 mph). (b) Relative change (%) between stages (and standard deviation) in median of normalized fuel consumption across all drivers (operating speed is 25 mph).

Figs. 14(a) and 14(b) also present the standard deviation of relative improvement on fuel consumption per distance across all drivers between stages. It can be observed from the figures that compared to Stage II, the "automated" driving performs much more robustly. In other words, the "automatic" driving can provide much higher fuel savings over Stage I but with much less variations. For example, as the operating speed changes from 20 mph to 25 mph, the standard deviation of relative fuel reductions (on average) provided by Stage II driving (over Stage I driving) vary from 15.2% to 18.5%, while the standard deviation range due to the introduction of Stage III is only between 6.3% and 9.0%. In addition, Stage I is (on average) less variant than Stage II, which may result from the more disturbing driving behaviors caused by the DVI assistance. Another interesting find is that the standard deviation of relative improvement in fuel consumption is usually high for those scenario boundary cells (e.g., "Green 12" cells for 25 mph in Table I), due to the fact that the situations in these cells are very sensitive to the driver's behavior (e.g., reaction time, capability to follow the driving guidance).

2) Mobility: Besides the fuel consumption and pollutant emissions, mobility performance (in terms of trip time) are also compared across different stages at different operating speeds. As shown in Table II, the average trip time of Stage III ("automated" driving) is slightly less than that of the "median" driver at Stage I ("manual-uninformed" driving), while the "median" driver at Stage II ("manual-DVI-assisted" driving) performed the worst, i.e., the average trip time is the longest. A test cell-based comparison on Table II may reveal that most of the mobility benefits of Stage III result from the cells (i.e., the blue cells) where "speed-up and pass" scenarios occurred, compared to the "full-stop" scenarios of "manual" driving.

B. Scenario-Based Comparison

Most drastic changes in performance measures for the same stage occur at boundary cells between different scenarios. In addition, the majority of benefits (in terms of environmental sustainability and mobility) of Stage III lie in those cells whose scenarios are different from "manual" driving. A comparison between scenarios (i.e., aggregation of associated cells in Table I and Table II) of related stages may provide more in-depth understanding on the performance of both "automated" and "manual" driving.

Tables III and IV summarize the results for fuel consumption and trip time on a scenario basis (column-wise combination), where cells that experienced the associated scenarios are

TABLE II
MEDIAN OF TRIP TIME (ACROSS ALL DRIVERS) FOR EACH TEST CELL (SECOND)

Speed (mph)	Phase	Green						Red						Avg.
	TIP	2	7	12	17	22	27	2	7	12	17	22	27	
20	I	32.5	32.5	62.5	57.0	52.0	47.5	42.0	37.0	33.0	32.5	33.0	33.5	41.3
	II	34.5	49.0	62.0	58.0	52.5	47.5	43.0	35.5	34.5	34.5	33.5	34.5	43.3
	III	35.0	33.0	27.0	60.0	57.0	50.0	46.0	39.0	35.0	35.0	35.0	36.0	40.7
25	I	27.0	27.5	59.5	56.0	50.0	46.5	41.0	36.0	30.0	27.5	27.0	27.0	37.9
	II	27.0	27.5	60.5	56.0	51.0	46.5	42.0	36.5	28.5	28.0	28.0	27.0	38.2
	III	28.0	28.0	22.0	59.0	56.0	50.0	46.0	38.0	33.0	28.0	28.0	28.0	37.0

TABLE III
RELATIVE IMPROVEMENT (%) BETWEEN STAGES WITH RESPECT TO MEDIAN OF NORMALIZED FUEL CONSUMPTION (SCENARIO-BASED)

Speed (mph)	Stage	Scenario						
		1 vs 1	2 vs 1	2 vs 3	3 vs 1	3 vs 3	4 vs 3	4 vs 4
20	II vs I	–3.3	/	/	–82.4	4.8	27.6	/
	III vs I	8.8	7.9	35.5	/	/	29.3	/
	III vs II	11.7	/	40.2	/	/	21.7	26.0
25	II vs I	5.9	/	/	/	5.9	/	34.7
	III vs I	17.5	/	39.1	/	/	13.4	31.0
	III vs II	12.3	/	32.8	/	/	8.7	–5.6

TABLE IV
RELATIVE IMPROVEMENT (%) BETWEEN STAGES WITH RESPECT TO MEDIAN OF TRIP TIME (SCENARIO-BASED)

Speed (mph)	Stage	Scenario						
		1 vs 1	2 vs 1	2 vs 3	3 vs 1	3 vs 3	4 vs 3	4 vs 4
20	II vs I	–4.3	/	/	–50.8	–0.8	4.1	/
	III vs I	–7.0	–1.5	56.8	/	/	–7.0	/
	III vs II	–2.6	/	45.9	/	/	–6.0	–9.9
25	II vs I	–1.1	/	/	/	–1.2	/	5.0
	III vs I	–2.9	/	63.0	/	/	–8.5	–10.0
	III vs II	–1.8	/	63.6	/	/	–7.3	–15.8

aggregated and relative changes (%) are then calculated. As can be observed from Tables I and II, for example, in cell "Green 12" at the operating speed of 25 mph, the "automated" driving is experiencing Scenario 2 while the "median" driver at Stage I and Stage II is experiencing Scenario 3. The improvements in fuel economy and trip time for the "automated" driving can be as high as 40% and 64%, respectively. This will contribute to the values (35.5% and 40.2%) in Table III where the Stage row is "III vs. I" or "III vs. II" while the column is "2 vs. 3" in Scenario (at 20 mph). If "automated" driving is experiencing Scenario 4 while "manual" driving is experiencing Scenario 3 (e.g., the cells from "Green 17" to "Red 2" at different operating speeds), then reduction in fuel consumption may range from 9% to 29% (depending on both stage and operating speed). It is noted that there are some increases in trip time. The hypothesis is that the departure trajectories in Stage III are much smoother (i.e., less aggressive acceleration and stable under automated control) than Stage I or II, even though the starting speeds of Stage III are a bit higher than those of Stage I or II when leaving the intersection at the start of green with compromise of mobility. The smoother acceleration profile for departure contributes to the increase in trip time for "automated" driving stage.

VI. CONCLUSION AND FUTURE WORK

In this study, the GlidePath Prototype system was developed and its performance was evaluated through extensive field experiments and comparisons with manual driving (both "uninformed" and "DVI-assisted"). By integrating connected vehicle technology with vehicle automation, the GlidePath Prototype system has exhibited great potential in reducing the vehicle's fuel consumption when traveling through the signalized intersection. The results show fuel savings of around 17% on average, with actual savings depending on the operating speed, the status of SPaT when engaging the system, and the availability of driving assistance. In contrast, use of DVI alone (Stage II) improved fuel economy over uninformed driving (Stage I) by only 5% on average, with a wide range of responses (18% standard deviation). Different drivers responded to the DVI differently, giving a wide range of fuel economy results. Through the use of automated longitudinal control, Stage III fuel economy results were much more consistent. When the "speed-up" scenarios are applicable, the GlidePath Prototype system (Stage III) is able to significantly improve mobility in addition to fuel efficiency. However, in other scenarios (especially the "glide" scenarios), the trip times of GlidePath Prototype system may be longer, because of the smoother trajectories (compared to manual driving with and without assistance) were deployed during the departure. It should be noted that in our testing, the vehicle could only reliably receive SPaT messages from the DSRC-equipped intersection within 190m (upstream) due to the blockage by trees and vertical curve effects of the testbed. Higher benefits may be expected, if the GlidePath Prototype system can start to take effect at a further distance (e.g., 300 m which is a nominal DSRC range) upstream from the signalized intersection.

The comparative analysis results also indicate that there are still research gaps in the area of driver-vehicle interface design. Although the core algorithm (i.e., eco-friendly vehicle trajectory planning) is the same as in the GlidePath Prototype system, the performance of "DVI-assisted" driving is not as good as anticipated (especially at the operating speed of 20 mph). A

more user-friendly design of DVI should be developed to how and when information should be disseminated to the driver. In addition, further improvement in the GlidePath Prototype system should be performed to guarantee its effectiveness in a variety of real-world situations (e.g., operation in mixed traffic under actuated signal control).

Besides, the integration of cooperative maneuvers among multiple connected vehicles (e.g., platooning via vehicle-to-vehicle communication) with different automation levels capabilities may result in some compound benefits. Another interesting research topic would be to develop an automated Eco-Approach and Departure system for a signalized corridor (e.g., multiple instrumented intersections with actuated signal timing) using long-range communication technologies such as the cellular network. From the perspective of near-term deployment, the validation of the proposed system (combined with preceding vehicle detection from e.g., a front radar, as shown in [14]) in a mixed traffic environment (with both connected and non-connected vehicles) should be an immediate next step.

ACKNOWLEDGMENT

The authors would like to thank the staff at the TFHRC for facilitating the field experiments. The authors would also like to thank Dr. Q. Jin for her contribution in data cleaning and Dr. G. Scora for his constructive comments.

REFERENCES

[1] European Commission, "eCoMove – Cooperative mobility systems and services for energy efficiency." [Online]. Available: http://www.ecomove-project.eu/
[2] European Union, "Compass4D – One step closer to C-ITS deployment in cities." [Online]. Available: http://www.compass4d.eu/
[3] U.S. Department of Transportation, "Applications for the environment: Real-Time Information Synthesis (AERIS)." [Online]. Available: http://www.its.dot.gov/aeris/
[4] *U.S. Department of Transportation*, Washington, DC, USA, "AERIS concept of operations and modeling workshop," Mar. 2013.
[5] B. Asadi and A. Vahidi, "Predictive cruise control: Utilizing upcoming traffic signal information for improving fuel economy and reducing trip time," *IEEE Trans. Control Syst. Technol.*, vol. 19, no. 3, pp. 707–714, May 2011.
[6] G. De Nunzio, C. Canudas De Wit, P. Moulin, and D. Di Domenico, "Eco-Driving in urban traffic networks using traffic signal information," in *Proc. 52nd IEEE Conf. Decis. Control*, Florence, Italy, Dec. 2013, pp. 892–898.
[7] M. Seredynski, B. Dorronsoro, and D. Khadraoui, "Comparison of Green Light Optimal Speed Advisory (GLOSA) approaches," in *Proc. 16th IEEE Conf. Intell. Transp. Syst.*, 2013, pp. 2187–2192.
[8] R. Kamalanathsharma and H. Rakha, "Agent-based simulation of eco-speed controlled vehicles at signalized intersections," *Transp. Res. Rec.*, vol. 2427, pp. 1–12, 2014.
[9] Z. Chen, Y. Zhang, J. Lv, and Y. Zou, "Model for optimization of eco-driving at signalized intersections," *Transp. Res. Rec.*, vol. 2427, pp. 54–62, 2014.
[10] National Highway Traffic Safety Administration, "Preliminary statement of policy concerning automated vehicles." [Online]. Available: http://www.nhtsa.gov/staticfiles/rulemaking/pdf/Automated_Vehicles_Policy.pdf
[11] G. Wu, K. Boriboonsomsin, H. Xia, and M. Barth, "Supplementary benefits from partial vehicle automation in an eco-approach and departure application at signalized intersections," *Transp. Res. Rec.*, vol. 2424, pp. 66–75, 2014.
[12] H. Yang, H. Rakha, and M. V. Ala, "Eco-cooperative adaptive cruise control at signalized intersections considering queue effects," *IEEE Trans. Intell. Transp. Syst.*, vol. 18, no. 6, pp. 1575–1585, Jun. 2017, doi: 10.1109/TITS.2016.2613740.
[13] M. Barth *et al.*, "The development of a comprehensive modal emissions model," NCHRP Web-Only Document 122, Contractor's Final Rep. NCHRP Project 25-11, Nat. Cooperative Highway Res. Progr., NAS Transport. Res. Board, Washington DC, Apr. 2000, p. 307.
[14] P. Hao, G. Wu, K. Boriboonsomsin, and M. Barth, "Developing a framework for eco-approach and departure application for actuated signal control," in *Proc. 2015 IEEE Intell. Veh. Symp.*, 2015, pp. 796–801.
[15] S. Mandava, K. Boriboonsomsin, and M. Barth, "Arterial velocity planning based on traffic signal information under light traffic conditions," in *Proc. 12th IEEE Conf. Intell. Transp. Syst.*, 2009, pp. 1–6.
[16] H. Rakha and R. Kamalanathsharma, "Eco-driving at Signalized Intersections Using V2I Communication," in *Proc. 14th IEEE Conf. Intell. Transp. Syst.*, 2011, pp. 341–346.
[17] M. Barth, S. Mandava, K. Boriboonsomsin, and H. Xia, "Dynamic ECO-driving for arterial corridors," in *Proc. 2011 IEEE Forum Integr. Sustain. Transp. Syst.*, 2011, pp. 182–188.
[18] K. S. Yi and J. T. Chung, "Nonlinear brake control for vehicle CW/CA systems," *IEEE/ASME Trans. Mechatronics*, vol. 6, no. 1, pp. 17–25, Mar. 2001.
[19] P. J. Huber, *Robust Statistics*. Hoboken, NJ, USA: Wiley, 1981.
[20] TORC Robotics. [Online]. Available: http://torcrobotics.com/pinpoint/
[21] SAE International, "Dedicated Short Range Communications (DSRC) message set dictionary." [Online]. Available: http://standards.sae.org/j2735_201603/
[22] E. Ozatay *et al.*, "Analytical solution to the minimum fuel consumption optimization problem with the existence of a traffic light," *ASME 2012 5th Annu. Dyn. Syst. Control Conf. Joint With JSME 2012 11th Motion Vib. Conf.*, 2012, pp. 837–846.
[23] E. Ozatay *et al.*, "Analytical and numerical solutions for energy minimization of road vehicles with the existence of multiple traffic lights," in *Proc. 52nd IEEE Conf. Decis. Control*, 2013, pp. 7137–7142.
[24] X. He, H. Liu, and X. Liu, "Optimal vehicle speed trajectory on a signalized arterial with consideration of queue," *Transp. Res. Part C, Emerg. Technol.*, vol. 61, pp. 106–120, Dec. 2015.
[25] Q. Jin, G. Wu, K. Boriboonsomsin, and M. Barth, "Power-based optimal longitudinal control for a connected eco-driving system," *IEEE Trans. Intell. Transp. Syst.*, vol. 17, no. 10, pp. 2900–2910, Oct. 2016.
[26] A. Garcia-Castro, A. Monzon, C. Valdes, and M. Romana, "Modeling different penetration rates of eco-driving in urban areas: impacts on traffic flow and emissions," *Int. J. Sustain. Transp.*, vol. 11, no. 4, pp. 282–294, 2017.
[27] M. Miyatake, M. Kuriyama, and Y. Takeda, "Theoretical study on eco-driving technique for an electric vehicle considering traffic signals," in *Proc. 2011 IEEE 9th Int. Conf. Power Electron. Drive Syst.*, Singapore, 2011, pp. 733–738.
[28] J. Hu *et al.*, "Integrated optimal eco-driving on rolling terrain for hybrid electric vehicle with vehicle-infrastructure communication," *Transp. Res. Part C, Emerg. Technol.*, vol. 68, pp. 228–244, Jul. 2016.

Osman D. Altan (LM'12) received the B.Sc. degree in electrical engineering from Middle East Technical University (METU), Ankara, Turkey, and the M.Sc. and Ph.D. degrees in electrical and computer engineering from the University of California, Berkeley, CA, USA. He worked in the Space Sciences Laboratory on scientific satellite systems launched by NASA for data acquisition. After briefly teaching at universities, he spent most of his career at General Motors Research and Development Center specializing on active safety systems, automated systems, and connected systems. He has 18 patents on related subjects and contributed to the company's launch of commercial products on safety, and comfort and convenience systems. Later, he joined the U.S. DOT's VOLPE Center in Cambridge, MA, USA, working on performance requirements of safety systems based on connectivity, and automated vehicle projects. He is currently with the U.S. DOT's Turner Fairbank Highway Research Center, McLean, VA, USA, managing several projects related to connected automation.

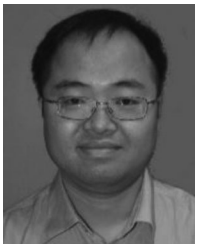

Guoyuan Wu (M'09–SM'15) received the Ph.D. degree in mechanical engineering from the University of California, Berkeley, CA, USA, in 2010. He currently holds an Assistant Research Engineer position in the transportation systems research group at Bourns College of Engineering—Center for Environmental Research & Technology, University of California at Riverside, Riverside, CA, USA. His research interests include development and evaluation of sustainable and intelligent transportation system technologies including connected and automated transportation systems, optimization and control of vehicles, and traffic modeling and simulation. He is a member of the Vehicle-Highway Automation Committee (AHB30) of the Transportation Research Board. He is also a board member of the Chinese Institute of Engineers Southern California Chapter and a member of the Chinese Overseas Transportation Association.

Matthew J. Barth (M'90–SM'00–F'14) received the B.S. degree in electrical engineering/computer science from the University of Colorado, Denver, CO, USA, in 1984, and the M.S. and Ph.D. degrees in electrical and computer engineering from the University of California, Santa Barbara, CA, USA, in 1985 and 1990, respectively. He is the Yeager Families Professor in the College of Engineering, University of California at Riverside (UCR), Riverside, CA, USA. He is part of the intelligent systems faculty in Electrical Engineering and is also serving as the Director for the Center for Environmental Research & Technology, UCR's largest multidisciplinary research center. He joined the University of California at Riverside in 1991, conducting research in intelligent systems. His research focuses on applying engineering system concepts and automation technology to transportation systems, and in particular how it relates to energy and air quality issues. His current research interests include ITS and the environment, transportation/emissions modeling, vehicle activity analysis, advanced navigation techniques, electric vehicle technology, and advanced sensing and control.

He is active with the U.S. Transportation Research Board serving in a variety of roles in several committees, including the Committee on ITS and the Committee on Transportation Air Quality. He was awarded the TRB Pyke Johnson Award for TRB outstanding paper in 2007. In 2011, he was one of the winners of the Connected Vehicle Technology Challenge sponsored by the U.S. Department of Transportation's Research and Innovative Technology Administration. He has also served on a number of National Research Council Committees. He has also been active in the IEEE Intelligent Transportation System Society for many years, participating in conferences as a presenter, invited session organizer, session moderator, reviewer, Associate Editor of the IEEE TRANSACTIONS ON INTELLIGENT TRANSPORTATION SYSTEMS, and member of the IEEE ITSS Board of Governors. He was the IEEE ITSS Vice President for Conferences from 2011 to 2012, President-Elect for 2013, IEEE ITSS President for 2014–2015, Past President in 2016, and Vice President for Finances for 2017. He received the IEEE ITS Society's Outstanding Research Award in 2016.

Kanok Boriboonsomsin (M'14) received the Ph.D. degree in transportation engineering from the University of Mississippi, Oxford, MS, USA, in 2004. He is currently an Associate Research Engineer in the College of Engineering—Center for Environmental Research & Technology, University of California at Riverside, Riverside, CA, USA. His research interests include sustainable transportation systems and technologies, intelligent transportation systems, traffic simulation, traffic operations, transportation modeling, vehicle emissions modeling, and vehicle activity analysis. He serves as an Associate Editor for the *IEEE Intelligent Transportation Systems Magazine*. He is a member of the Transportation and Air Quality Standing Committee of Transportation Research Board, Institute of Transportation Engineers, and the Intelligent Transportation Society of America.

John A. Stark received the B.S. degree in aeronautical engineering and the M.S. degree in mechanical engineering both from Purdue University, Lafayette, IN, USA, in 1982 and 1984, respectively. He is a Chief Software Engineer at Leidos (formerly SAIC), Reston, VA, USA, where he has been employed for 20 years. He has been working under contract to the FHWA on various connected and automated vehicle research and development projects since 2014. Prior to that, he worked on development and maintenance of various military systems. Prior to employment with SAIC, he worked for 11 years at McDonnell Douglas Aerospace in software and mechanical engineering capacities. He was a Licensed Professional Engineer for 15 years.